

Synergistic action in colloidal heat engines coupled by non-conservative flows

Sudeesh Krishnamurthy,¹ Rajesh Ganapathy,^{2,3} and A. K. Sood^{1,2}

¹*Department of Physics, Indian Institute of Science, Bangalore - 560012, INDIA*

²*International Centre for Materials Science,*

*Jawaharlal Nehru Centre for Advanced Scientific Research,
Jakkur, Bangalore - 560064, INDIA*

³*Sheikh Saqr Laboratory, Jawaharlal Nehru Centre for Advanced Scientific Research,
Jakkur, Bangalore - 560064, INDIA*

(Dated: January 19, 2021)

Abstract

Colloidal microspheres in optical tweezers are model systems for mesoscopic particles in conservative harmonic potentials and are used to realize micrometer-sized heat engines. While non-conservative forces and hydrodynamic flows that dissipate energy input by them are known to exist, their effect on the motion of the colloidal bead in an isolated optical trap has been shown to be negligible. Here, we demonstrate that the same, however, is not true if another particle is trapped in close proximity. The internal energy of the adjacent trapped colloid gets enhanced by obstructing the flows generated by non-conservative forces and in turn feeds it back to the microsphere. We establish this specifically in the case of two colloidal beads trapped in close separation and the synergy between them was observed predominantly along the direction of laser propagation. Using parameters that tune the hydrodynamics, we showed that the energy addition can in turn be controlled. Leveraging on these results in a manner analogous to microswimmers that increase propulsion velocity by collectively exploiting non-conservative flows, we operated two micrometer sized heat engines constructed from the colloidal microspheres and showed that their performance can be similarly enhanced. The increased performance was observed to arise by reusing the energy input otherwise rejected into the hydrodynamic flows. While these results explore only the simplest case of two engines, the underlying concepts should be considered while designing larger collections. Nevertheless, our results mark the first basic step towards constructing engines by a bottom-up architecture akin to biological systems.

The development of micrometer sized heat engines [1–7] over the past decade has enabled the reinterpretation of the laws of classical thermodynamics in a fluctuation dominated regime. A paradigmatic system used in such realizations consists of a colloidal microsphere - the working gas, in a focused laser beam that confines the particle like a piston. Thermodynamic cycles are executed by synchronized variations in intensity of the beam and temperature of the suspending medium. Engine realizations hitherto [1, 2] assumed that the optical forces exerted on the microsphere are conservative and the surrounding medium acts as a thermal bath. In principle, however, non-conservative forces are also exerted on the colloidal particle due to light scattering at the microsphere-water interface [8–12]. The resulting circulations in the probability flux termed - Brownian vortexes - could locally drive the bath out of equilibrium. Nevertheless, under isotropic conditions, where the trapped microsphere is sufficiently isolated from other particles and is at a significant distance from the boundaries of the system [13], deviations due to such effects are negligible. Experimental studies in the past have also investigated the origins of the deviations when such symmetries are violated, in particular, due to trapping close to an interface along the z -direction [14]. Under such conditions, the hydrodynamic flows due to the Brownian vortexes were restricted by the presence of a surface and in turn affected the particle motion. Alternately, a surface that constrains the vortexes could also be created by trapping another colloidal particle in close proximity - a situation encountered when constructing collections of engines with multiple microspheres [15]. The ensuing vortexes in such a case would bring about non-trivial couplings and lead to co-operative behavior between the particles. Inducing hydrodynamic interactions by affecting the non-conservative flow fields - a hallmark feature of colonies of microswimmers [16–18] could then be emulated in collections of optically trapped microspheres. Although realizing such collections of engines by generating multiple optical traps is straightforward with holographic tweezers [19, 20], the extent to which the non-conservative forces affect their performance remains to be quantified.

Here, we observe the operation of two heat engines, the simplest case of collective behavior and quantified the effects of non-conservative forces as they are brought close to each other. Our system consists of two colloidal microspheres trapped in adjacent optical harmonic potentials created by a pair of tightly focused laser beams as sketched in Fig. 1a. The optical potentials L_1 and L_2 were formed by focusing laser beams with mutually perpendicular polarizations at a distance d from each other, in which, colloidal microspheres of diameter σ

are trapped. The intensity gradient created by a focused laser is known to apply conservative forces [21] on dielectric particles with refractive index different from the surrounding medium and forms the most dominant force in the system. For the Gaussian beams used in our experiment, these forces are harmonic as illustrated in the Fig. 1a. Nevertheless, the same refractive index difference also results in laser scattering from the microsphere-solution interface, and as a consequence, in a finite non-conservative force [10–12] along the direction of propagation. The optical energy input to the bead by the scattering force is dissipated by viscous damping into the thermal energy of the surroundings. In steady state, these forces result in probabilistic circulatory motion of the particle called Brownian vortices [8, 9]. As noted earlier, under isotropic conditions, despite the correlated dynamics due to the ensuing hydrodynamic flows, the feedback of the energy into particle motion has been estimated to be negligible [13]. However, large scale particle motions could ensue if they are hindered by an interface, particularly in the z -direction [14]. In our experiments, the colloidal particle in the adjacent trap provides such an interface and we exploit this to bring about a non-trivial coupling between the two particles.

To ascertain the effects due to the restriction of vortex flows, we observed the probability distribution of particle motion in L1 and L2. Fig. 1b shows change in the probability density of particle positions, $\delta\rho(r, z)$ of a colloidal bead trapped in L1 when another identical microsphere is introduced in L2 and vice-verse for two distances of separation $d = 3.6\mu\text{m}$ and $4.8\mu\text{m}$. $\delta\rho(r, z)$ is projected on the r - z plane of the cylindrical co-ordinates, $\mathbf{r} = (r, \phi, z)$ with the laser propagation direction as the $+z$ axis. The particle positions were measured relative to the mean position of the bead in the isolated trap. $\rho(r, z)$ spreads to larger values of r and z on mutual interaction, indicating an energy transfer, E_t to the particle motion. Majority of the increase in circulation, as can be seen from the Fig. 1b, occurs along the direction of laser propagation, the z -axis, where the trap stiffness is the least. The change in the mean position of $\rho(r, z)$, however, was $\approx 5 - 10\text{nm}$ and negligible within the limits of the tracking resolution. Since the optical fields L1 and L2 remain constant during the observations in Fig. 1b, $\delta\rho(r, z)$ is necessarily due to inter-particle interaction. The screening length of the electrostatic potential of the colloidal particle in our suspending medium, 10 mmol NaCl is $\approx 10\text{nm}$, while the least surface separation between the beads used in our experiments was $1.6\mu\text{m}$. Since the counter-ions in the suspending salt solution tightly screen surface charges on the colloid, the change in $\rho(r, z)$, cannot occur due to the electrostatic double layer

interactions. Further, although the motion of trapped colloidal particles is anti-correlated [22] (See supplementary Fig. S1), hydrodynamic transfer of thermal energy between the two traps in equilibrium reservoirs is prohibited by exchange fluctuation theorem [23]. Also, the increase in temperature due to laser absorption was estimated to be $\approx 0.1 - 0.2K$ [24]. Thus, change in $\rho(r, z)$, cannot be due to thermal convection currents. Also, Casimir forces between the two microspheres operate in length scales $\approx 100nm$ [25] and do not affect $\rho(r, z)$. Thus, the source of change in $\rho(r, z)$ is due to the interplay between the probabilistic flows generated by the trapped particles.

To demonstrate that the probabilistic flows are sufficient to generate the required energy addition, we observed the changes in $\delta\rho(r, z)$ with variations in bath temperature, T which mainly results in significant changes in viscosity of the solution, μ while the refractive index, n remains constant. This in turn affects only the flow mediated interactions such as those generated by Brownian vortexes. We quantified the feedback of energy to the particle motion, E_t by integrating potential energy along z-direction over the change in the probability density as

$$E_t = \frac{1}{2} \int k_z \delta\rho(r, z) z^2 r dr dz \quad (1)$$

where, k_z is the trap stiffness along the z-axis. Since maximum change in $\rho(r, z)$ occurred along the direction of propagation, potential energy change in the x-y plane was found to be very small $\approx 5 - 10\%$ of that along z-axis and was neglected in our calculations. In Fig. 2a, we measure E_t at two temperatures $T_H = 313K$ and $T_C = 290K$ as total incident laser power $S = S(L1) + S(L2)$ was varied, while the ratio of the intensities $S(L2)/S(L1) = 1.33$ was maintained constant. The viscosity $\mu(T_C) = 1.08mPa \cdot s$ was 1.7 times that of $\mu(T_H) = 0.65mPa \cdot s$, while the refractive index of the medium, n changed only in the fourth significant digit from $n(T_C) = 1.325$ to $n(T_H) = 1.323$. Thus, across the two temperatures, the dynamical properties of the medium were different, but the optical forces experienced by the bead remained the same. The variation of E_t with S in both L1 and L2 was observed to be significantly different across the two temperatures (Fig. 2a) and verifies that the probabilistic flows are sufficient to produce the energy addition. The trends in E_t can be intuitively anticipated from the asymptotic behavior of the vortexes with S . At any given T , for a sufficiently large S , the conservative harmonic potential generates the most dominant force in the system and all vortexes should cease to exist. As a consequence, E_t should decrease with S . Alternately, at low k , where the particle explores a significant

volume, increasing S results in more scattering and larger swirls that enhance E_t . The crossover between these behaviors is dictated by parameters such as viscosity, refractive index. Similar crossovers in particle dynamics have also been observed in previous studies [9, 26] on isolated optical traps with k_z in the same range as those used in our experiment. But the k_z at which they occur is harder to predict due to the chaotic nature of the vortices. As observed in our experiment, due to lower viscosity, circulation lies below the crossover at T_H and above for T_C . Thus, temperature essentially acts as a switch for viscosity with which the energy addition from Brownian vortices can be modulated. Further, to demonstrate that these flows are necessary for energy addition, we measure the changes in E_t with d , along which the vortices are known to decay. As can be seen from Fig. 2b, E_t decreases sharply as d increases beyond 2-3 particle diameters at both T_H and T_C . Thus, the probabilistic flows are necessary and sufficient to produce the energy addition.

To further obtain a visual confirmation on the central role of the underlying vortices in the energy addition, we observe their influence on the motion of the trapped particle. In Fig. 3, we plot the streamlines of velocity field of the trapped microsphere in the r - z plane at $S = 125mW$ and $T = 313K$, where maximum E_t was observed in our experiments. Displacements of the particle calculated over equal intervals of time $\approx 2ms$ were spatially averaged over boxes of size $5nm \times 10nm$ to form an average velocity field and plotted as streamlines in Fig. 3. Such an averaging provides us a glimpse of the particle motion in the absence of thermal noise. Intuitively, in such a scenario, particles released in the extremities should trace the streamlines and converge to the center of the trap at $(r, z) = (0, 0)$, a stable fixed point had there been only conservative forces. In the presence of non-conservative forces and the associated hydrodynamic flows, however, similar to the findings in earlier literature [9], we observed that they converged to a region close to the $z=0$ plane, but at finite r , even in isolated optical traps as shown in Fig. 3a. Streamlines in this region develop into circulatory vortex patterns akin to strange attractors due to the chaotic hydrodynamic flows. In Fig. 3b, we plot the resultant streamlines on addition of a particle to the adjacent trap. We observe that the microspheres released from extremities could remain significantly farther from the $z=0$ plane and small changes in their initial position could result in very distinct trajectories. Thus, introducing a trapped particle in close proximity results in an increase in chaotic hydrodynamic flows that lead to energy addition by mutual interaction as anticipated by our observations. The difference in E_t between $T = 313K$ and $T = 290K$

at $S = 125mW$ can also be similarly expected by comparing the circulatory patterns before inserting a particle to the neighboring trap (See Supplementary Fig. S2).

We now exploit the non-trivial coupling between the microspheres to affect the operation of a pair of engines at close separation. In the absence of such a coupling, since the working gas - colloidal particle in both the engines are in equilibrium with the same reservoir, heat flow between them is prohibited by the zeroth law of thermodynamics. Thus, irrespective of the separation between the engines, their performance would remain the same. However, in the presence of non-conservative forces, as established above, the microspheres extract energy from the vortexes of the particle trapped in close proximity, which would otherwise be rejected into the reservoir if they were well separated. This additional energy input could drive the reservoir out of equilibrium and lead to a better performance.

With colloidal particles in both the optical traps L1 and L2, we executed the microscopic equivalent of Stirling cycle [1–3] (See supplementary movie) for various distances of separation. The isothermal processes were performed by changing the total laser power, S between $(S_{max}, S_{min}) = (71mW, 125mW)$ as the temperature of the suspending medium was maintained constant. The isochoric processes were realized by passing heat exchanging fluid in an adjacent channel [3], which modulates the temperature between $(T_H, T_C) = (313K, 290K)$ as S is maintained constant. The engines are operated synchronously without any phase difference with a cycle time of $22s$ ($7s$ for each isotherm and $4s$ for each isochore). As relaxation times for hydrodynamic transfer of energy between the microspheres is $\approx 10ms$, the engines are effectively operated in the quasi-static limit. Since the engine bath interactions at small d would now include the mutual interaction between the flows generated by Brownian vortexes, which depend on S , the effective protocol by the engine deviates, particularly along the isotherms from the Stirling cycle. Nevertheless, to compare the performance across various d , we followed the same protocol at all d as for $d = \infty$. The performance of the engine in these realizations at various d (rescaled by σ) are plotted in Fig. 4. The work done and efficiency were calculated by tracing the particle trajectories and using the framework of stochastic thermodynamics [3, 27, 28]. Since the diameter of the trapping laser beam at the focal point was $\approx 500nm = \sigma/4$, the non-conservative part of the optical potential was confined to a region less than the size of the microsphere and is independent of the separation between the particles. Thus, as in the case of isolated optical traps, we considered only the dominant conservative harmonic potential to calculate the

thermodynamic quantities. Due to the variation of S in the isothermal cycles, the stiffness of this potential varied between $(k_{zmin}, k_{zmax}) = (0.41 \pm 0.02, 0.58 \pm 0.01)pN/\mu m$ for L1 and $(k_{zmin}, k_{zmax}) = (0.56 \pm 0.01, 0.795 \pm 0.02)pN/\mu m$ for L2. From the Fig. 4a, we see that the average total work done by the engine, $\langle W(L1 + L2) \rangle$ measured from trajectories along all the three axes x,y and z, in units of $k_B T_C$ increase sharply along with the individual work done by both the traps $\langle W(L1) \rangle$ and $\langle W(L2) \rangle$, as $\sigma/d \rightarrow 1$. As a result of this, the average total efficiency $\epsilon(L1 + L2)$ plotted in Fig. 4b also increases simultaneously. Most of this enhancement in performance, however, occurs when L1 and L2 are closer than 2-3 particle diameters, as can be seen from the dotted lines drawn to capture this trend.

To isolate the contribution from the changes in vortexes, we plot the average work done along the z-direction, $\langle W_z \rangle$ measured in units of $k_B T_C$ for the individual traps in Fig. 4c. As can be seen from the figure, $\langle W_z \rangle$ increases by 3.5 times as the engines are brought into close proximity. About 70% of this occurs at separation distances in the range of 2-3 particle diameters, where, as described in Fig. 2b energy is input into the particle motion from the vortexes. Thus, most of the increase in $\langle W(L1 + L2) \rangle$ can be attributed to the increase in $\langle W_z \rangle$. As a result of this, the efficiency calculated along the z-axis, ϵ_z for both L1 and L2 (Fig. 4d) increase drastically by about 3 times and the increase in $\epsilon(L1 + L2)$ can be attributed to the better performance of the engine along the z-axis.

To elucidate the origins of increase in the performance of the engines due to operation at close proximity, we trace the trajectory of the system in the state space of the Stirling cycle - the k-T plane. However, an effective temperature that describes the fluctuations in the system can be defined only when the probability distribution of the particle position, $P(\Delta z)$ resemble those due to a thermal reservoir, i.e. follow a Gaussian profile for our harmonic optical trap [29]. A system with an additional non-equilibrium noise, as in our experiment, follows such a distribution only if either the potential is sufficiently wide, or amplitude of the active fluctuations are significantly small. To verify if even one of this holds true in our case, we plot $P(\Delta z)$ in Fig. 5a for L2 at k_{max} with a bath temperature at T_H , where, maximum E_t was detected in our setup (Fig. 2a). Deviations from an ‘Equilibrium-like’ behavior, if any, should show up under these extreme conditions. As established earlier (Fig. 1b), we observe that the $P(\Delta z)$ widens on interaction (Fig. 5a). The solid lines which represent Gaussian fits to $P(\Delta z)$ match well with the experimental measurements only in the first decade but deviate from the fit in the tails. The increase in the energy encompassed

by the Gaussian fits measured by averaging potential energy across the distribution [3] was found to be about $\approx 0.41k_B T_C$. This accounts for only 72% of the total E_t associated with the entire $P(\Delta z)$. Thus, the synergistic action simultaneously affects both, the width and the statistics of the system. This is in contrast with observations in earlier literature [8] in isolated traps, where, $P(\Delta z)$ was shown to be Gaussian. Thus, the coupling of the vortexes causes a significant input of energy into the particle motion. Nevertheless, a T_{act} derived from the potential energy of the system can still be defined by following protocols in previous studies on active engines [3], using equipartition theorem $\frac{1}{2}k_B T_{act} = \frac{1}{2}k_z \langle z^2 \rangle$. As in the case of E_t , we consider motion only along the z-direction to calculate T_{act} , since the addition of another particle in the adjacent trap causes negligible changes in $P(\Delta x)$ and $P(\Delta y)$ (Fig. 1b, also see Supplementary Fig. S3).

We can now plot the state of the system on the $k_z - T_{act}$ plane as shown in Fig. 5 b and c. As anticipated from Fig. 2a, the coupling between the particle motion results in deviations from the effective Stirling protocol. Since E_t has a strong dependence on S , significant deviations were observed along the isotherms, where, S is adjusted to vary the trap stiffness/confinement, k_z at constant bath temperature, T . As a consequence, the path traced by the system is no longer a rectangle, but a distorted trapezoid. Although the area in the $k_z - T_{act}$ plane increases on coupling (Fig.s 5 b and c), it does not necessarily represent the work done. Nevertheless, the difference in T_{act} between the hot and cold 'isotherms' is proportional to work done and increases on introducing the adjacent particle. Thus, distortions of the effective Stirling protocol lead to enhancement of the work done and efficiency. The source of the performance, however, is not just the energy added by the neighboring trap, but the difference in the increase in T_{act} between the hot and cold reservoirs, which in-turn depends crucially on the nature of the vortexes. While processes that involve reusing the energy rejected by the adjacent trap can be captured in a minimal model by adding a dissipative term, A_{jizj} to the Langevin equation (See supplementary information), a detailed knowledge of the hydrodynamic flows is necessary to elucidate the increase in performance. In conclusion, we have exploited the non-conservative forces in focused laser beams, to bring about a non-trivial coupling between two micrometer sized colloidal heat engines. The total performance of the engines increased due to the energy addition from the associated flows due to Brownian vortexes when they were operated in close proximity. Although such vortexes existed even in isolated traps, the optical energy input

from the non-conservative forces was rapidly dissipated into the surroundings. Our results demonstrate that in the presence of a neighboring particle, this energy can be reused to extract work. Thus, even though the energy input remains the same, if engines that generate non-conservative flows are operated in close vicinity, they utilize the same energy intake better. While the nature of vortices in the general case of a large collection of microspheres might be harder to analyze, our results establish that unlike isolated engines, the non-conservative couplings between them could influence the total performance. Hydrodynamic flows generated by non-conservative forces are also characteristic to all microswimmers [16–18] and self-propelled particles [30] driven by electric and magnetic fields [31–34], chemical reactions [35, 36] etc. Interactions in collections of such particles are also mediated by the hydrodynamic flows [16–18, 35, 37, 38]. It would be tempting to consider that the superior performance observed in our experiments could also be a reflection of the enhancement of propulsion velocity observed in collections of such microswimmers [16–18, 34, 35].

In conclusion, we have exploited the non-conservative forces in focused laser beams, to bring about a non-trivial coupling between two micrometer sized colloidal heat engines. The total performance of the engines increased due to the energy addition from the associated flows due to Brownian vortices when they were operated in close proximity. Although such vortices existed even in isolated traps, the optical energy input from the non-conservative forces was rapidly dissipated into the surroundings. Our results demonstrate that in the presence of a neighboring particle, this energy can be reused to extract work. Thus, even though the energy input remains the same, if engines that generate non-conservative flows are operated in close vicinity, they utilize the same energy intake better. While the nature of vortices in the general case of a large collection of microspheres might be harder to analyze, our results establish that unlike isolated engines, the non-conservative couplings between them could influence the total performance. Hydrodynamic flows generated by non-conservative forces are also characteristic to all microswimmers [16–18] and self-propelled particles [30] driven by electric and magnetic fields [31, 34], chemical reactions [35, 36] etc. Interactions in collections of such particles are also mediated by the hydrodynamic flows [16–18, 35, 38]. It would be tempting to consider that the superior performance observed in our experiments could also be a reflection of the enhancement of propulsion velocity observed in collections of such microswimmers [16–18, 34, 35].

MATERIALS AND METHODS

The polystyrene colloidal microspheres (mean diameter, $\sigma = 2.03\mu m$) used for realization of the heat engine in our experiment were obtained from Bangslabs, USA. The particles were trapped in 10mmol NaCl solution at a distance of $25\mu m$ from the surface of a coverslip by tightly focusing a NDYVO4 IR laser beam of wavelength, $\lambda_0 = 1064nm$ with a Carl Zeiss 100X objective with numerical aperture, N.A. = 1.4 mounted on a Carl Zeiss Axiovert Microscope. While trapping in a salt solution prevented double layer interactions between the particles, the sufficiently large distance from the coverslip avoided boundary effects on the system. To create two adjacent optical traps, we split the incident laser beam into perpendicularly polarized components using a polarizing beam splitter, which were then independently steered into the back aperture of the objective. Since, the vortexes created by the non-conservative forces is sensitive to parameters such as orientation of the beams, difference between their intensities, position of the focus etc., the steering process would create two distinct optical traps, despite being operated at the same power. In our experiments, however, we maintained the ratio between the intensities at $S(L2)/S(L1) = 1.33$ and studied the most general case of the coupling. The beam waist at the focal point, which indicates the region of influence of the laser was $\approx \frac{2\lambda_0}{\pi N.A.} = 480nm$ and significantly lesser than the closest separation distance between the microspheres $\approx 3.6\mu m$ used in our experiment. To mark the end points of the isochoric process and to monitor the distance from the coverslip, a very low powered red laser (Thorlabs ML101J8 Diode laser of wavelength 632 nm controlled using a Thorlabs TCLDM9 temperature controlled laser diode module) aligned at a slanting angle was shined at a distance at least $10\mu m$ from the trapped particles. The red laser was switched on only during the isochoric processes and its reflection from the bottom coverslip of the sample cell was monitored. This provided us the necessary temporal resolution to resolve the isochoric process as well as spatial resolution of $0.2\mu m$ to monitor the distance from the coverslip. The solution temperature was tuned by flowing heat exchanging fluid in an adjacent chamber used in earlier experiments on active engines [3]. Particles were imaged using a Basler Ace 180 kc color camera at 500frames/sec . The influence of red laser was eliminated by considering only the green slice of the RGB image and the particle position is tracked to sub-pixel resolution to an accuracy of 5 nm along x-y and 10 nm along z direction using custom built tracking codes in Matlab.

ACKNOWLEDGEMENTS

AKS and SK thank the Department of Science and Technology, India for financial support under the Year of Science Professorship and Nanomission council.

- [1] V. Bickle and C. Bechinger, *Nature Physics* **8**, 143 (2012).
- [2] I. A. Martínez, É. Roldán, L. Dinis, D. Petrov, J. M. Parrondo, and R. A. Rica, *Nature physics* **12**, 67 (2016).
- [3] S. Krishnamurthy, S. Ghosh, D. Chatterji, R. Ganapathy, and A. Sood, *Nature Physics* **12**, 1134 (2016).
- [4] J. Roßnagel, S. T. Dawkins, K. N. Tolazzi, O. Abah, E. Lutz, F. Schmidt-Kaler, and K. Singer, *Science* **352**, 325 (2016).
- [5] J. V. Koski, V. F. Maisi, J. P. Pekola, and D. V. Averin, *Proceedings of the National Academy of Sciences* **111**, 13786 (2014).
- [6] O. Abah, J. Rossnagel, G. Jacob, S. Deffner, F. Schmidt-Kaler, K. Singer, and E. Lutz, *Physical review letters* **109**, 203006 (2012).
- [7] A. Dechant, N. Kiesel, and E. Lutz, *Physical review letters* **114**, 183602 (2015).
- [8] Y. Roichman, B. Sun, A. Stolarski, and D. G. Grier, *Physical review letters* **101**, 128301 (2008).
- [9] B. Sun, J. Lin, E. Darby, A. Y. Grosberg, and D. G. Grier, *Physical Review E* **80**, 010401 (2009).
- [10] A. Ashkin, *Biophysical journal* **61**, 569 (1992).
- [11] S. Sukhov and A. Dogariu, *Reports on Progress in Physics* **80**, 112001 (2017).
- [12] P. Wu, R. Huang, C. Tischer, A. Jonas, and E.-L. Florin, *Physical review letters* **103**, 108101 (2009).
- [13] G. Pesce, G. Volpe, A. C. De Luca, G. Rusciano, and G. Volpe, *EPL (Europhysics Letters)* **86**, 38002 (2009).
- [14] M. Khan and A. Sood, *Physical Review E* **83**, 041408 (2011).
- [15] B. J. De Cisneros and A. C. Hernández, *Physical review letters* **98**, 130602 (2007).

[16] K. Drescher, R. E. Goldstein, N. Michel, M. Polin, and I. Tuval, Physical Review Letters **105**, 168101 (2010).

[17] R. Ledesma-Aguilar and J. M. Yeomans, Physical review letters **111**, 138101 (2013).

[18] C. Pooley, G. Alexander, and J. Yeomans, Physical review letters **99**, 228103 (2007).

[19] J. E. Curtis, B. A. Koss, and D. G. Grier, Optics communications **207**, 169 (2002).

[20] E. R. Dufresne, G. C. Spalding, M. T. Dearing, S. A. Sheets, and D. G. Grier, Review of Scientific Instruments **72**, 1810 (2001).

[21] A. Ashkin, J. M. Dziedzic, J. E. Bjorkholm, and S. Chu, Optics letters **11**, 288 (1986).

[22] J.-C. Meiners and S. R. Quake, Physical review letters **82**, 2211 (1999).

[23] A. Bérut, A. Imparato, A. Petrosyan, and S. Ciliberto, Physical review letters **116**, 068301 (2016).

[24] E. J. Peterman, F. Gittes, and C. F. Schmidt, Biophysical journal **84**, 1308 (2003).

[25] J. L. Garrett, D. A. Somers, and J. N. Munday, Physical review letters **120**, 040401 (2018).

[26] B. Sun, D. G. Grier, and A. Y. Grosberg, Physical Review E **82**, 021123 (2010).

[27] K. Sekimoto, Progress of Theoretical Physics Supplement **130**, 17 (1998).

[28] U. Seifert, Reports on progress in physics **75**, 126001 (2012).

[29] J. Palacci, C. Cottin-Bizonne, C. Ybert, and L. Bocquet, Physical Review Letters **105**, 088304 (2010).

[30] C. Bechinger, R. Di Leonardo, H. Löwen, C. Reichhardt, G. Volpe, and G. Volpe, Reviews of Modern Physics **88**, 045006 (2016).

[31] A. Bricard, J.-B. Caussin, N. Desreumaux, O. Dauchot, and D. Bartolo, Nature **503**, 95 (2013).

[32] M. Trau, D. Saville, and I. A. Aksay, Science **272**, 706 (1996).

[33] A. S. Negi, K. Sengupta, and A. Sood, Langmuir **21**, 11623 (2005).

[34] J. Buzhardt and P. Tallapragada, Physical Review E **100**, 033106 (2019).

[35] P. Bayati and A. Najafi, The Journal of chemical physics **144**, 134901 (2016).

[36] A. A. Solovev, S. Sanchez, and O. G. Schmidt, Nanoscale **5**, 1284 (2013).

[37] F. Martínez-Pedrero, E. Navarro-Argemí, A. Ortiz-Ambriz, I. Pagonabarraga, and P. Tierno, Science advances **4**, eaap9379 (2018).

[38] M. Driscoll and B. Delmotte, Current opinion in colloid & interface science **40**, 42 (2019).

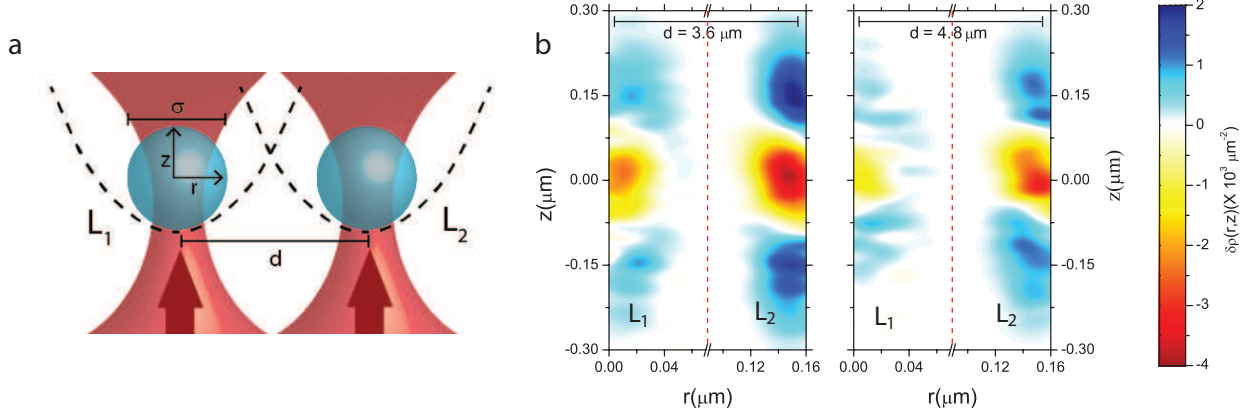


FIG. 1. **Schematic of the experimental setup.** **a** shows schematic of experimental setup. **b** denotes change in the probability density $\delta\rho(r, z)$ (represented by the scheme shown in the colorbar) on introduction of an identical bead in the adjacent trap for $d = 3.6\mu m$ and $4.8\mu m$. The total laser power $S = 125mW$ and $S(L2)/S(L1) = 1.33$ and the solution temperature was maintained at 313K. The distributions were obtained by binning $\approx 20,000$ particle positions over boxes of size $5\mu m \times 10\mu m$. The resulting distributions were further linearly interpolated onto boxes of size $0.5\mu m \times 0.5\mu m$ to obtain smoother profile.

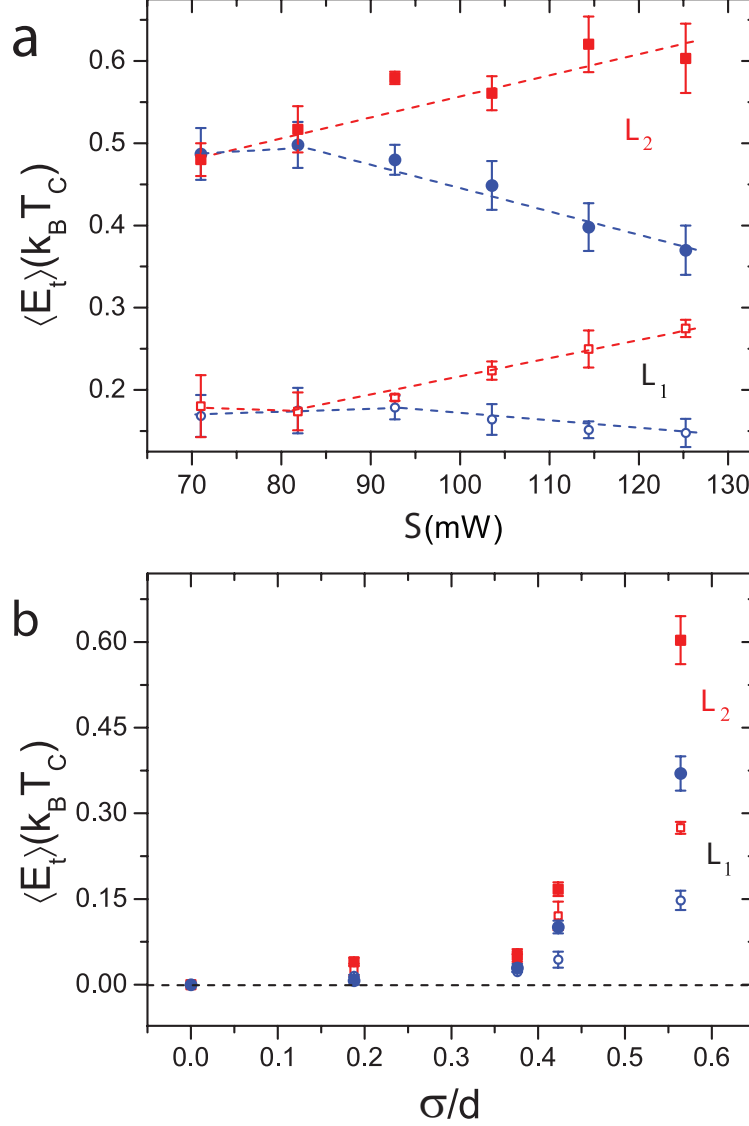


FIG. 2. **Characterization of non-conservative flows** **a** shows E_t , measured in units of $k_B T_C$, where k_B is the Boltzmann constant and $T_C = 290K$, for different total laser power, $S(L1 + L2)$ with $d = 3.6\mu m$ at two temperatures $T_H = 313K$ (red squares) and $T_C = 290K$ (blue circles) for both the traps L1 (open symbols) and L2 (closed symbols). $S(L2)/S(L1) = 1.33$ was maintained constant and the dotted lines are a guide to the eye. **b** E_t , at various σ/d for the maximum total laser power $S_{max} = 125mW$ and $\sigma = 2.03\mu m$. E_t at two temperatures T_H (red squares) and T_C (blue circles) are plotted for both the traps L1 (open symbols) and L2 (closed symbols). The error bars represent standard error of mean over three independent realizations

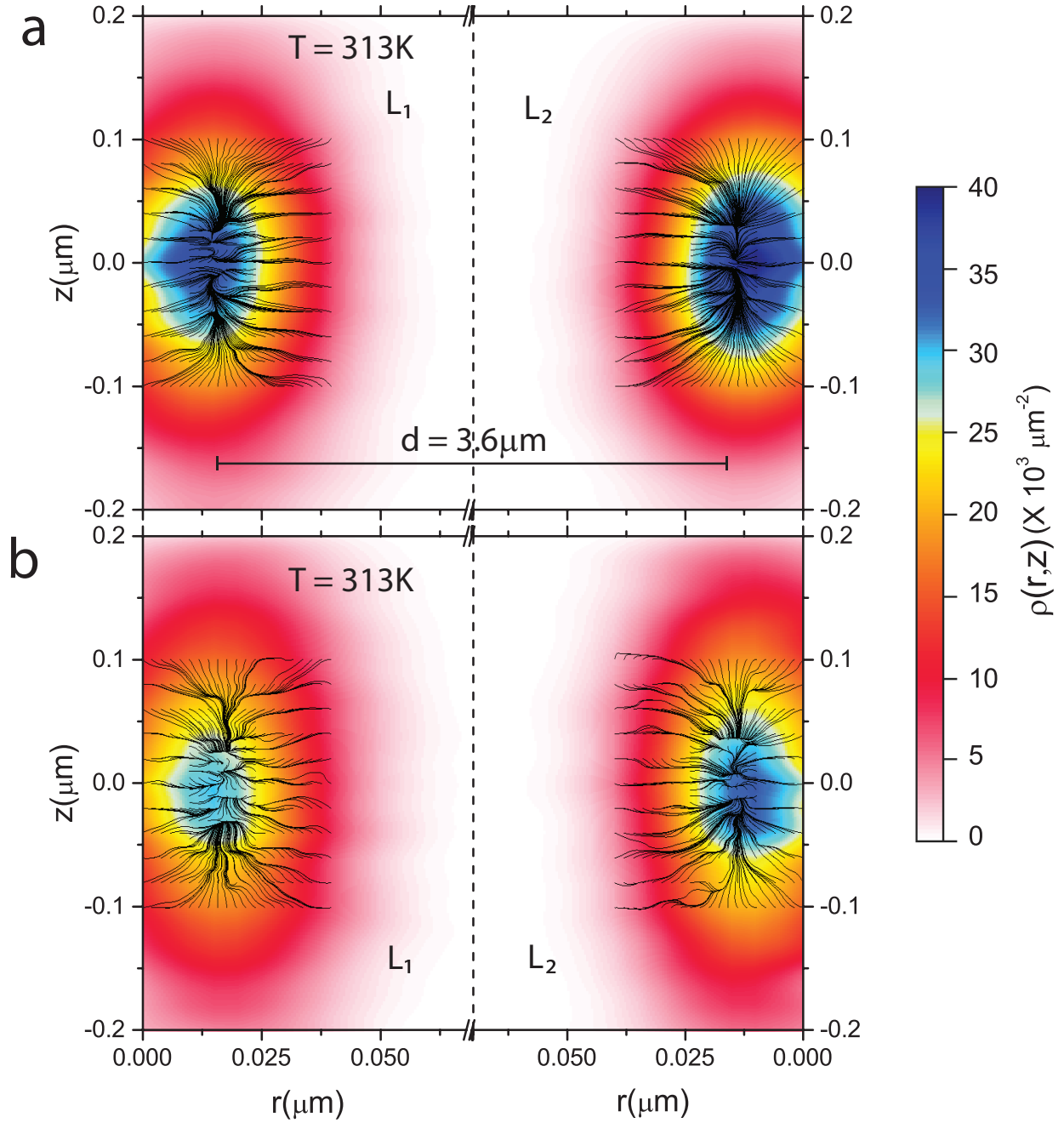


FIG. 3. **Vizualization of non-conservative flows** **a** shows streamlines of average particle displacement plotted in the r - z plane for both L_1 and L_2 for an isolated trap at $T = 313K$ with $S = S_{max} = 125mW$ and $S(L2)/S(L1) = 1.33$. The background image represents the probability density of the particle, $\rho(r,z)$ color coded as shown in the color bar. **b** represents the same on addition of an identical bead in the adjacent trap at $d = 3.6\mu\text{m}$.

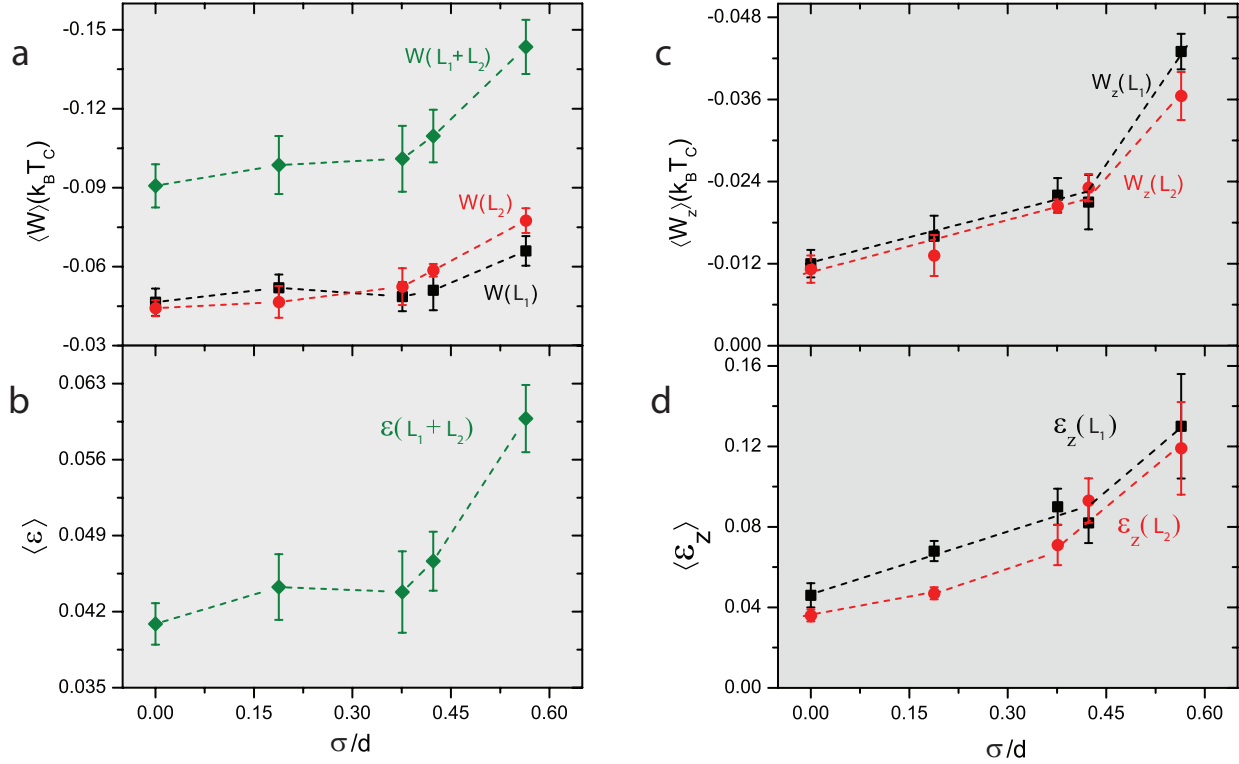


FIG. 4. **Performance of the engine on coupling** **a** shows $\langle W(L_1 + L_2) \rangle$ (green diamonds), $\langle W(L_1) \rangle$ (Black squares) and $\langle W(L_2) \rangle$ (Red circles) in units of $k_B T_C$ for various separation distances d rescaled by σ . **b** demonstrates $\langle \epsilon(L_1 + L_2) \rangle$ (green diamonds) for the same. The dotted lines are a guide to eye drawn to capture the change in the trend as L_1 and L_2 are brought closer than 2-3 particle diameters. **c** and **d** represent similar contributions from the engine along the z -direction. The error bars represent standard error of mean over ≈ 150 cycles.

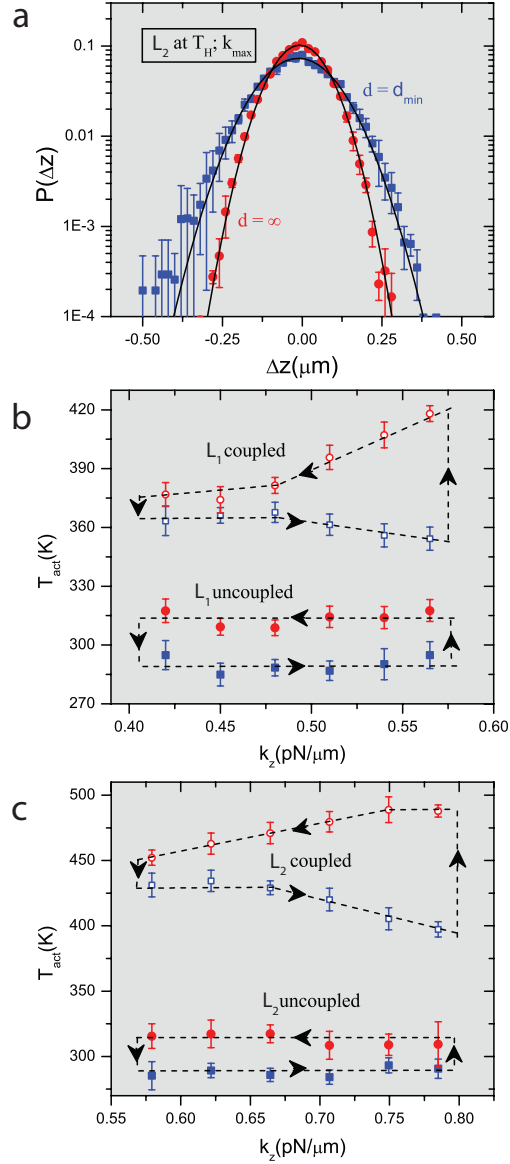


FIG. 5. **Elucidating the origins of superior performance.** **a** $P(\Delta z)$ of a particle in L2 before(red squares) and after(blue circles) addition of another colloidal bead in L1 for $T = T_H$, $d = d_{\min} = 3.6\mu\text{m}$ and $k = k_{\max}$, where, the largest E_t was observed in Fig 3, is plotted. The solid lines represent Gaussian fits for the same. **b** and **c** show the trajectory of the system in the $k_z - T_{\text{eff}}$ plane for the engine in L1 and L2 respectively as Stirling cycle is performed before(white filled symbols) and after(color filled symbols) introducing an identical particle in the adjacant trap. In the above experiments $d = d_{\min} = 3.6\mu\text{m}$, $T_H = 313\text{K}$ (Red circles) and $T_C = 290\text{K}$ (Blue squares). The error bars are standard error of mean over three independent realizations.